Estimation of $AvAl_2O_3$ and $RxSiO_2$ by Partial Least Square Regression (PLSR) on XRD data: A Case Study Using Low Grade Bauxites

Caio César A. Melo[1] and Simone P. A. Paz[1,2]
1. Programa de Pós-Graduação em Engenharia de Recursos Naturais da Amazônia (UFPA).
2. Laboratório de Caracterização Mineral, Instituto de Geociências, Universidade Federal do Pará, Campus do Guamá, 66075-110, Belém, Pará, Brasil
Corresponding author: eng.caiomelo@hotmail.com

Abstract

Wet chemistry used for grade control of bauxites is an industry standard for quantification of available alumina ($Av Al_2O_3$) and reactive silica ($Rx SiO_2$), but very costly and time-consuming. Alternative methods for these determinations are constantly studied with the aim of providing speed and practicality. In this work, X-ray diffraction data using the statistical tool of Partial Least Square Regression (PLSR) analysis was used to predict the amount of available alumina and reactive silica, related to gibbsite and kaolinite respectively, in several samples of four bauxite lithologies from the Paragominas Mine in Pará State, Northern Brazil. Rietveld refinement was carried out in some of the analyzed samples and both estimates were compared with wet chemistry data. Results have shown that it was possible to achieve a good prediction of reactive silica content, even for those bauxites with higher silica content. The quality of XRD data required for prediction applying PLSR is also discussed. The tool has proven to be very powerful in predicting these values, and it may be an alternative for the grade control of bauxites.

Keywords: bauxite, reactive silica, partial least square regression, powder XRD.

1. Introduction

The production of bauxite is increasing every year, and as reported by U.S. Geological Survey [1] world production reached about 300 Mt in 2017, where more than 90 % is refined by the Bayer process. In this scenario, Brazil plays an important role, having the 4th largest deposits and production in the world. Brazilian bauxites are concentrated mainly in the Amazon region, more specifically in the state of Pará, where about 35.7 million tonnes of bauxite are produced per year, representing more than 93 % of the national production [2].

One of the greatest challenges faced by the alumina industry is the high levels of reactive silica ($Rx SiO_2$) in bauxites, which leads to a costly loss of caustic soda during Bayer refinery processing [3]. Due to the formation of insoluble sodium-alumino-silicate phases (DSP – Desilication Product), the more $Rx SiO_2$ present in the bauxite, the more caustic soda is lost in the process as fixed soda in the solid residue. Despite the amount of available alumina ($Av Al_2O_3$), the presence of high $Rx SiO_2$ results in many of the world's reserves of bauxite being sub-economic.

The high levels of $Rx SiO_2$ in some of Brazilian bauxites, such as those from Paragominas (in the Miltonia region of the State of Pará, Northern Brazil), require good quality control to ensure that the ore fed to the Bayer process is within the acceptable limits of $Av Al_2O_3$ and $Rx SiO_2$, avoiding economic penalties. Currently, the grade control relies on the consolidated wet chemistry methods [4]. Such methods consist of simulating the Bayer process on a laboratory scale and then determining the levels of $Av Al_2O_3$ and $Rx SiO_2$, providing indirectly the approximate contents of gibbsite and kaolinite respectively [5, 6]. Apart from their known accuracy and uncertainty, these traditional methods are time-consuming and demand a large quantity of

chemicals, manpower and laboratory space [4, 7]. In addition, it is essential to know the mineralogy and texture of the minerals, since these determine the physicochemical interactions occurring in the processes. There are no guarantees that only the wet chemical determinations will allow high efficiency control in the metallurgical processes [7, 8].

Other methods have been proposed for mineralogical classification and quantification of bauxites based on statistical tools and X-ray diffraction data [4, 6, 7, 9, 10]. These methods are proposed as fast, practical and relatively reliable alternatives for obtaining bauxite mineralogy, for optimizing the operation of mining and processing plant.

Since the pioneer works on partial least square (PLS) by Wold [11], this method has become widely used in many fields of applied science like chemometrics, bioscience and social science [12, 13, 14]. As stated by Geladi E Kowalski [15] PLS is a good alternative to multiple linear regression (MLR) and principal component regression (PCR) methods due its robustness. Such methods are well suited when data is strongly collinear, and the numbers of variables is greater than observations, which is common for analytical data such as UV-visible, infra-red and Raman spectra and XRD patterns [16, 17, 18].

The PLS method provides a prediction of hidden information (latent variables) from the raw data, which can be of great interest for industrial process control. The advances in XRD detectors allows obtaining good quality data within a few minutes [14, 18]. In this context, application of the PLS method directly to the XRD raw data appears to be an interesting alternative for the industrial grade control of ores and processes [14, 19, 20]. This study aimed to evaluate the applicability of the PLS regression on XRD data of several bauxite samples, including low grade samples (high silica content) to predicting the principal parameters required for process control.

2. Experimental

2.1. Materials

A total of 64 samples of bauxites were used, randomly selected from sampling boreholes at the Miltonia 3 plateau. Both the samples and the quantification their extractables ($Av Al_2O_3$ and $Rx SiO_2$) were provided by Hydro Paragominas. According to the typical lateritic profile of the plateau, the samples correspond to four lithologies: BN (Nodular Bauxite), BNC (Nodular/Crystalized Bauxite), BC (Crystalized Bauxite) and BCBA (Crystalized/Amorphous Bauxite). More details of borehole sampling, localization and grid size, sample preparation, and description of the lithologies are given in Melo et al [10] and Silva et al [21].

2.2. XRD data

The powder XRD data were collected using a PANalytical *Empyrian* diffractometer, equipped with a θ-θ goniometer, Co X-ray tube ($K\alpha_1$ = 1.78901 Å), Fe Kβ filter and a PIXel^{3D} 2x2 area detector (linear scanning mode) with active length of 3.3473º 2θ (255 channels). Analyses were carried out under the follow conditions: 40 kV and 35 mA; soller slit of 0.04 rad; ¼ º and ½ º divergent and anti-scattering slits respectively; 0.02 º 2θ step size; sample spinning with 1 rotation per second. Two scan ranges and time per step were adopted resulting in different times of measurements (Table 1). The main idea was to optimize the measurement time while maintaining a good prediction.

Rietveld refinement was performed using the PANalytical software HighScore Plus v7.4. The CIF files were: 6162 – Gibbsite; 87771 – Kaolinite; 170915 – Hematite; 109411 – Al-Goethite; and 202242 – Anatase. Background was fitted for each XRD pattern and the following

parameters were refined: sample displacement, scale factor, unit cell and profile-shape (pseudo-Voigt function). More attention was paid to the parameters: profile function "U, V and W" and preferred orientation (March-Dollase function), mainly for gibbsite, and eventually for kaolinite. Samples were refined differently depending on the content of these two phases. All refinements converged for agreement parameters R_{exp}, R_{wp}, and GOF lower than 3.50, 9.00, and 2.95 respectively. All values of R_{exp}, R_{wp}, GOF and the R_{Bragg} for gibbsite and kaolinite are summarized in the appendix.

Table 1. Operating conditions for the XRD data collection.

Scan range (º 2θ)	Time per step (s)	Measurement time	Condition of XRD data collection*
5 – 70	27.54	5 min	A
	56.865	10 min	B
12 – 45	27.54	2 min 30 s	C
	56.865	5 min 30 s	D

**Nomenclature adopted throughout the text for the conditions of XRD data collection.*

2.3. Partial Least Square Regression (PLSR)

Partial Least Square Regression (PLSR) as well as several traditional chemical analyses consists, in general terms, of two steps: first a regression model is found that better fits the data and then a prediction is made for unknown samples using that model. The process divided the data matrix into a number of blocks (**X** – dependent and, **Y** – independent) which were modelled by principal components as outer relations (**X** = **TP'** + **E** and **Y** = **UQ'** + **F**; where **E** and **F** are the matrices of residuals). Simultaneously, an inner relation between the blocks are made by relations in the latent variables (**û = b.t**; **X** block score: **u** and, Y block score: **t**) [11, 15]. **X** generally is an inexpensive and/or fast measure, while **Y** is usually expensive, difficult and/or time-consuming. In practical application, one can easily make a prediction of any **Y** property having on hand only the **X** data.

PLSR was performed using the PANalytical software HighScore Plus v7.4. This software uses the SIMPLS algorithm proposed by de Jong [22] as an alternative to the NIPALS algorithm [11]. A detailed approach to the mathematics and algorithms involved in PLS regression can be found in [12, 13, 22, 23].

The calibration models were "trained" using 31 samples/datasets. The inputs were the bauxite XRD patterns (**X** matrix) and the *Rx*SiO_2 and *Av*Al_2O_3 results from the wet chemistry (**Y** matrix). Next, the models were tested on 33 samples/datasets to predict both the *Rx*SiO_2 and *Av*Al_2O_3.
To evaluate the precision and accuracy of the prediction, four samples from each lithology were prepared, measured by XRD and analyzed by PLSR five times in each condition. In addition, Rietveld refinement was performed on these samples and both prediction methods were compared. The results were analyzed by ANOVA.

3. Results and Discussion

The XRD pattern of all samples is shown in Figure 1. Mineralogical phases present in these bauxite lithologies are the same: kaolinite, gibbsite, hematite, Al-goethite and anatase. More details of characterization are given in Melo et al [10]. The region of the main *hkl* reflections of the hematite is highlighted in Figure 1. As observed, the background pattern is noticeably higher for samples with higher levels of iron minerals due to the fluorescence effect [24].

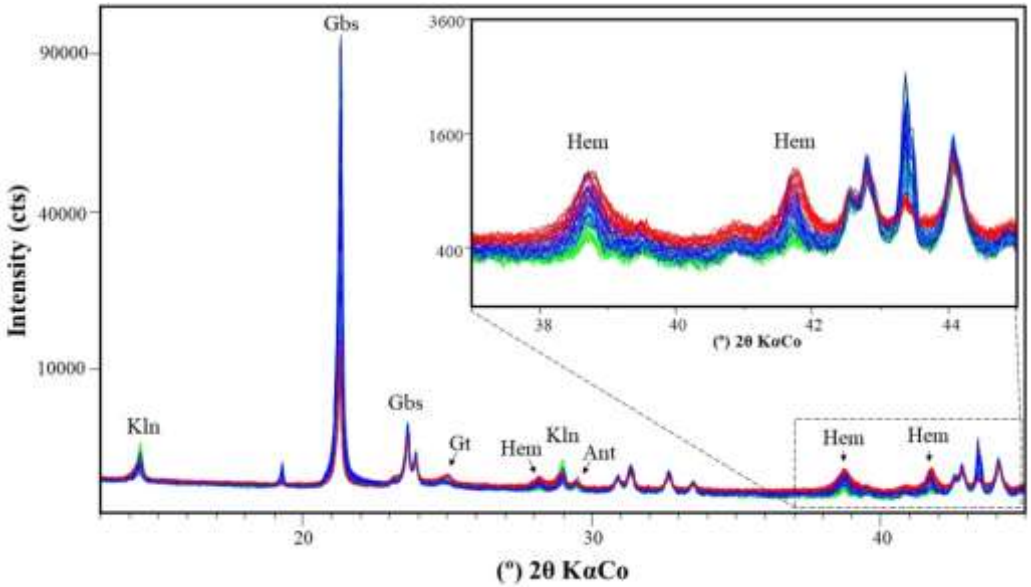

Figure 1. XRD patterns of all 64 bauxite samples.
Lithologies are grouped by colors: BN-red, BNC-aqua, BC-blue and, BCBA-lime).
Legend: Kln: kaolinite; Gbs: gibbsite; Gt: goethite; Hem: hematite; Ant: anatase.

3.1. PLSR analysis

The predicted model quality was evaluated for several conditions of data collection and processing. The approach of background subtraction for the PLSR of iron rich samples proposed by Webster et al [20] was applied in this study in an attempt to minimize differences in the datasets due to lithologies with distinct contents of iron minerals.

The calibration models were quickly and easily obtained using the PLSR tool in the HighScore Plus 4.7 software. The optimal number of factors, scaling mode and the RMSEP (root-mean-square error of prediction) were tested and calculated through a cross-validation (summarized in Table 2). The best scaling mode for the raw XRD dataset was "standardize" and "center" only for the condition A. When the background is subtracted, scaling the datasets by standardize mode has almost no effect regardless the number of PLSR factors (Figure 2a).

Table 2. PLS parameters of the selected calibration models by cross-validation.

	Condition of XRD data collection	*Av*Al_2O_3			*Rx*SiO_2		
		Scaling mode	RMSEP (%)	Nº of PLSR factors	Scaling mode	RMSEP (%)	Nº of PLSR factors
Raw XRD data	A	Center	0.804	8	Center	0.563	8
	B	Standardize	0.673	6	Standardize	0.482	5
	C	Standardize	0.716	5	Standardize	0.48	5
	D	Standardize	0.64	5	Standardize	0.459	6
Background Subtracted	A	Center	0.854	7	Center	0.584	7
	B	Center	0.834	8	Standardize	0.547	3
	C	Center	0.861	8	Center	0.611	7
	D	Standardize	0.717	5	Standardize	0.567	3

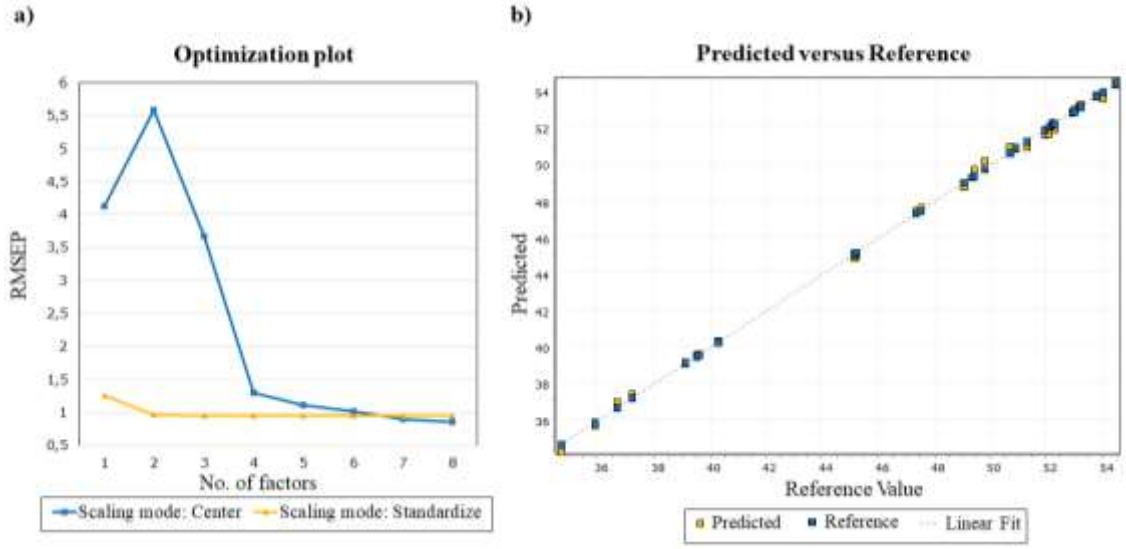

Figure 2. a) Optimization plot showing the tested scaling modes (RMSEP as function of the number of PLSR factors) – the low influence of standardize for background subtracted datasets; b) PLS fit for the calibration model (results from condition of XRD data collection "C" with background subtracted).

The RMSEP value is presented at the same unit of the Y dataset, therefore, the goodness-of-fit were satisfactory for all calibration models (Figure 2b). The delta value, representing the difference between wet chemistry and PLSR results are summarized in the Table 3 (full table given in the appendix). As observed, all conditions tested result in a good calibration model for both available alumina and reactive silica.

Table 3. Delta values from the Raw XRD calibration dataset obtained by cross-validation.

	A		B		C		D	
	AvAl_2O_3	*Rx*SiO_2	*Av*Al_2O_3	*Rx*SiO_2	*Av*Al_2O_3	*Rx*SiO_2	*Av*Al_2O_3	*Rx*SiO_2
No. of sample	**Delta**	**Delta**	**Delta**	**Delta**	**Delta**	**Delta**	**Delta**	**Delta**
1	0.235	-0.445	-0.009	-0.178	-0.066	-0.018	0.079	-0.02
2	0.021	0.062	-0.013	-0.013	-0.049	0	-0.076	0.009
3	0.048	-0.091	0.031	-0.017	-0.216	0.043	-0.127	-0.027
4	-0.343	0.127	-0.128	0.144	-0.114	0.005	-0.277	0.034
5	0.158	-0.033	-0.021	0.048	0.024	0.01	-0.047	0.027
6	-0.351	0.213	0.008	0.113	0.002	-0.031	-0.198	0.005
7	0.057	-0.03	0.029	-0.044	0.014	0.04	0.056	-0.043
8	0.133	-0.149	-0.067	-0.09	-0.04	0.05	-0.153	-0.012
9	-0.043	0.094	0.035	-0.049	0.082	-0.024	0.269	0.002
10	0.208	-0.038	-0.016	-0.12	-0.049	-0.022	0.261	0.059
11	0.19	-0.12	0.048	-0.089	0.055	-0.007	0.167	-0.002
12	0.057	-0.079	-0.04	0.031	-0.024	0.03	0.005	-0.03
13	0.188	-0.113	0.049	-0.114	0.188	-0.019	0.366	0.028
14	0.073	-0.027	-0.07	0.098	0.044	0.052	-0.063	0.057
15	-0.149	-0.012	-0.065	-0.028	0.003	-0.027	-0.177	-0.031
16	-0.142	0.048	-0.035	0.117	-0.093	-0.043	-0.292	-0.006
17	-0.372	0.234	-0.033	-0.113	0.011	-0.048	-0.092	-0.018
18	-0.174	0.169	-0.013	0.177	-0.071	0.006	0.001	0.048

19	-0.143	0.123	0.034	-0.056	0.125	-0.022	0.006	-0.01
20	0.132	-0.008	0.054	0.09	0.107	0.032	0.175	-0.031
21	-0.015	-0.21	0.034	-0.049	0.016	0.033	-0.075	-0.034
22	0.249	-0.047	-0.007	0.079	0.096	-0.019	0.215	0.019
23	0.104	-0.024	-0.054	-0.159	-0.034	-0.057	0.027	0.048
24	0.103	-0.069	0.101	-0.082	-0.06	0.026	-0.011	-0.092
25	0.165	-0.216	-0.011	-0.059	-0.015	-0.056	-0.244	-0.045
26	-0.314	0.234	-0.008	-0.026	-0.114	0.019	-0.069	0.009
27	0.003	-0.101	-0.009	-0.112	0.052	0.007	-0.132	0.009
28	-0.046	0.261	0.03	0.144	0.022	0.024	0.07	0.027
29	0.059	0.209	0.099	0.121	0.104	0.012	0.168	-0.008
30	-0.019	0.012	0.035	0.124	0.032	-0.019	0.216	0.048
31	-0.071	0.027	0.012	0.115	-0.034	0.024	-0.048	-0.019

3.2. Prediction of *Av*Al_2O_3 and *Rx*SiO_2

The quality of the PLSR prediction was measured by comparing its values with the wet chemistry results (Figure 3). Each condition of the predictor datasets was compared and the standard deviation of the responses analyzed. As observed in Figure 4, the prediction values were "biased" for each condition of the XRD data. The low standard deviation values confirm that all predictions were satisfactory. However, in this particular case, removing the background as proposed by Webster et al [20], implies a loss of prediction quality. This demonstrates that the levels of iron minerals in the ore and its effect on background, do not affect the quality of *Av*Al_2O_3 and *Rx*SiO_2 prediction.

In addition, best results for both response variables were found from the condition "D": reduced 2θ range (13º – 45º) and higher time per step (56.865 s). This means that an XRD pattern covering only the main *hkl* reflections of gibbsite and kaolinite is sufficient to provide valuable information for this process control. König et al [14] also support the idea of reducing the 2θ range, to increase the sample throughput without sacrificing accuracy. Webster et al [20] on the other hand, supports a thorough understanding of how rapid an XRD data may be, since cropping the XRD data in that case, reduced the correlation between the measured and calculated responses.

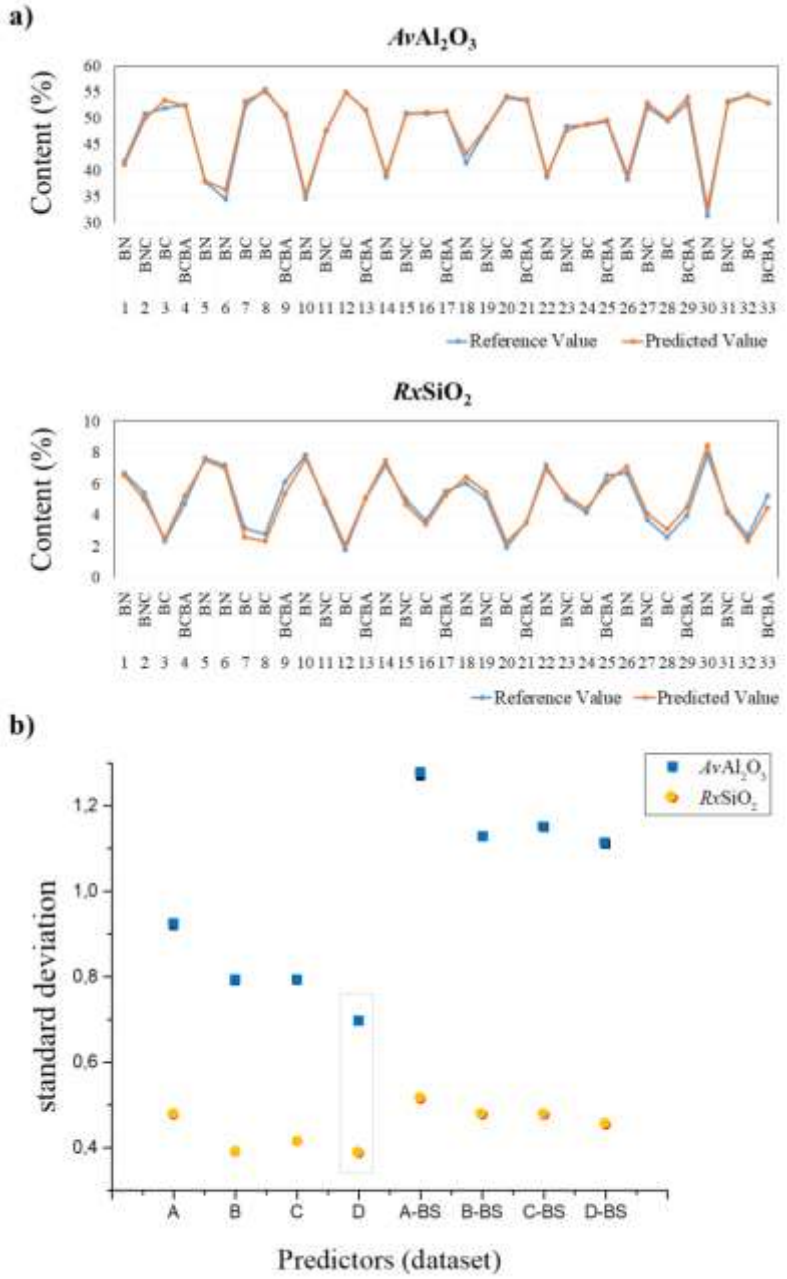

Figure 3. Comparison of wet chemistry and PLSR results for $Av Al_2O_3$ and $Rx SiO_2$. a) for a series of test samples using condition "D". b) Standard deviation of the predicted values as function of the XRD data conditions.

The correlation between wet chemistry and PLSR results for the condition "D" is presented in Figure 4. The high correlation observed for both estimations, in agreement with König et al [4], shows that XRD can be used to analyze bauxites, even with high diversity of the mineralogical phases and for low-grade ores.

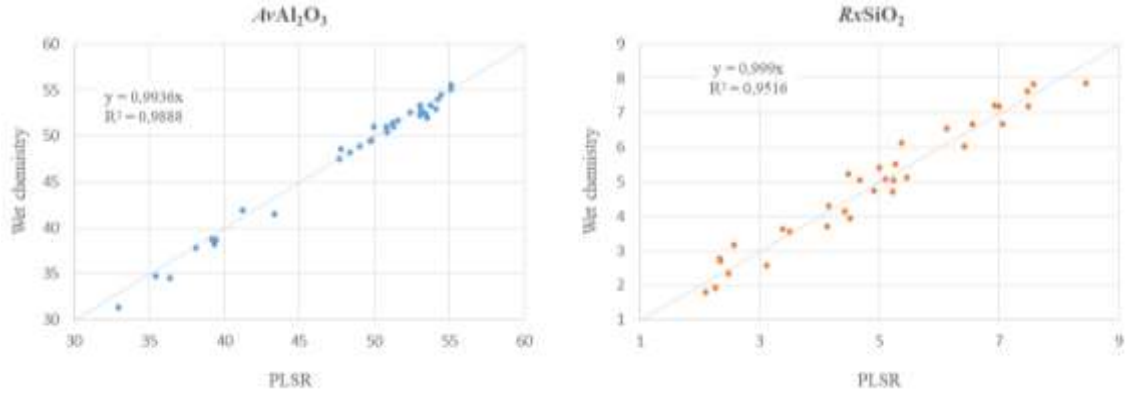

Figure 4. Correlation between PLSR and results from wet chemistry for available alumina and reactive silica using de XRD data condition "D".

3.3. Precision, Accuracy and Comparison with Rietveld Refinement

The precision of values obtained by the PLSR analysis were estimated by ANOVA. Table 4 summarizes the means and standard deviation (SD) of the differences between measured and calculated $Rx\text{SiO}_2$ and $Av\text{Al}_2\text{O}_3$ values.

Table 4. Measures of dispersion of the PLSR results.

	$Av\text{Al}_2\text{O}_3$		$Rx\text{SiO}_2$	
Lithology	**Mean**	**SD**	**Mean**	**SD**
BN	-1.794	0.773	-0.228	0.084
BNC	-0.142	0.546	-0.307	0.135
BC	-0.942	0.433	-0.824	0.178
BCBA	-0.740	0.492	0.195	0.144

These values are better represented in Figure 5 which clearly shows the precision (the small SD) and accuracy (how close the prediction is from delta = 0) of the $Av\text{Al}_2\text{O}_3$ and $Rx\text{SiO}_2$ estimation. Kaolinite present in lithology BN, besides being in large amounts (greater than 5 %), has the highest degree of structural disordering [10]. The broadening of *00l* reflections probably had an influence on the loss of accuracy of the $Rx\text{SiO}_2$ estimation.

For comparison, Rietveld refinement results are also presented in Figure 5. The prediction and standard deviation of $Av\text{Al}_2\text{O}_3$ and $Rx\text{SiO}_2$ are in good agreement with those reported in references [4, 6, 25]. However, the biggest problem faced with bauxite (preferred orientation), strongly affects the accuracy and especially the reproducibility of the method. This is particularly true for lithologies with high levels of gibbsite and kaolinite, BC and BCBA respectively. To reduce this effect, a new approach was proposed by Paz et al [7, 26] and Angelica et al [6]. In contrast, the PLSR method appears to be advantageous, since preferred orientation has no significant effect in the estimation.

It is noteworthy that this calibration model was purposely constructed with samples of high- and low-grade bauxite, to cover a wide range of available alumina and reactive silica contents. Better results would probably be achieved for process control using a dataset containing only those lithologies which represent commercial ore grades.

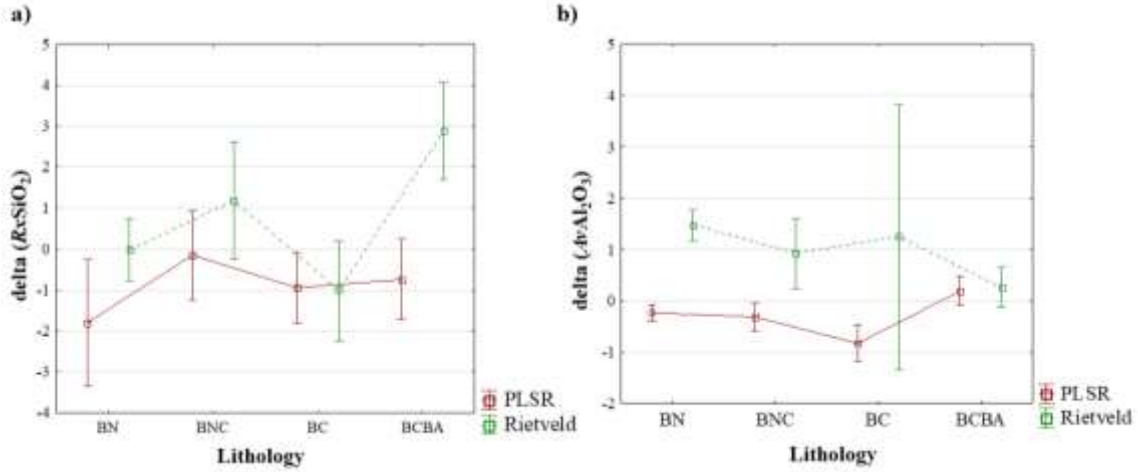

Figure 5. Plot of delta of PLSR and Rietveld prediction vs lithology. a) expressed for *Rx*SiO_2. b) expressed for *Av*Al_2O_3. *Bars denote the SD.*

4. Conclusions

Available alumina and reactive silica contents, the main parameters for grade control of bauxites, were successfully determined from several samples using the PLSR method directly from raw XRD data. It shows to be robust at the rapid prediction of wet-chemical determinations (*Av*Al_2O_3 and *Rx*SiO_2) from unknown samples.

The quality of the XRD data needed to achieve satisfactory predictions were evaluated. It was concluded that by reducing the scan range 2θ from 5 º – 70 º to 13 º – 45 º, the measurement time is optimized without loss of accuracy. The optimal conditions for XRD data collection were found to be: *scan range*: 3º – 45º (2θ), and *time per step*: 56.865 s. However, satisfactory results were obtained even for the measurement time of 2 min 30 s.

The model constructed using both high and low-grade bauxites allowed the prediction of *Av*Al_2O_3 and *Rx*SiO_2 values from all lithologies including those of marginal bauxites and gangues. This can improve process control in mining, streamlining communication between the laboratory and the mine, when there is a mineralogical change in the feedstock.

5. References

1. E. L. Bray. Bauxite and alumina. *Mineral Commodity Summaries*. USGS, (2018), 30–31.
2. Brasil. Departamento Nacional de Produção Mineral. *Sumário Mineral* / Coordenadores T. M. Lima, C. A. R. Neves. Brasília: DNPM, 2018, 131 p.
3. P. Smith. The processing of high silica bauxites – review of existing and potential processes. *Hydrometallurgy* Vol. 98, (2009),162–176.
4. Uwe König et al., Rapid X-ray diffraction (XRD) for grade control of bauxites. *International Committee for Study of Bauxite, Alumina & Aluminium – ICSOBA*, November 2012, Belém. Papers, Bauxite Program BX14-T, 11 p., CD-ROM.
5. S. Ostap. Control of silica in the Bayer process used for alumina production. *Can. Metall*. Vol. 25, (1986), 101–106.
6. R. S. Angélica, H. Kahn, S. P. A. Paz. A proposal for bauxite quality control using the combined Rietveld-Le Bail-Internal Standard PXRD method – Part 2: Application to a gibbsitic bauxite from the Paragominas region, northern Brazil. *Minerals Engineering*, Vol. 122, (2018), 148–155.

7. S.P.A. Paz, H. Kahn, R.S. Angélica, A proposal for bauxite quality control using the combined Rietveld – Le Bail – Internal Standard PXRD method – Part 1: *hkl* model developed for kaolinite. *Minerals Engineering* Vol. 118, (2018), 52–61.
8. D. J. O'Connor. Alumina Extraction from Non bauxitic Materials. *Aluminium Verlag*, Sydney, (1988), 370 p.
9. Bulent Tutmez, Bauxite quality classification by shrinkage methods. *Journal of Geochemical Exploration*. Vol. 191, (2018), 22–27.
10. C. C. A. Melo et al., Cluster Analysis from X-ray Diffraction data: A practical tool for mineralogical classification of bauxites and related products from the Bayer digestion. *Holos*, Vol. 6, (2017), 32–42.
11. H. Wold, Estimation of principal components and related models by iterative least squares, in P.R. Krishnaiah (Editor), *Multivariate Analysis*, Academic Press, New York, 1966, 391-420.
12. Agnar Höskuldsson. PLS regression methods. *Journal of Chemometrics.* Vol. 2, (1988), 221–228.
13. M. C. F. Ferraro, P. M. Castellano, T. S. Kaufman. A spectrophotometric-partial least squares (PLS-1) method for the simultaneous determination of furosemide and amiloride hydrochloride in pharmaceutical formulations. *Journal of Pharmaceutical and Biomedical Analysis*. Vol. 26, (2001), 43–451.
14. Uwe König, Thomas Degen, Nicholas Norberg. PLSR as a new XRD method for downstream processing of ores: – case study: Fe 2+ determination in iron ore sinter. *Powder Diffraction*. Vol. 29, (2014),
15. Paul Geladi, Bruce R. Kowalski. Partial least-squares regression: a tutorial. *Analytica Chimica Acta*. Vol. 185, (1986), 1–17.
16. S. Wold, et al., The collinearity problem in linear regression, the partial least squares approach to generalized inverses, *SIAM J. Sci. Stat. Comput.* Vol.5, (1984), 735–743.
17. S. Wold, M. Sjöström, L. Eriksson. PLS-regression: a basic tool of chemometrics. *Chemometrics and Intelligent Laboratory Systems*. Vol. 58, (2001), 109–130.
18. Thomas Degen et al., The HighScore suite. *Powder Diffraction*, Vol. 29, (2014) 13–18.
19. Uwe König, Nicholas Norberg, Process Control in Aluminium Industry – News in the XRD Tool Box. *Proceedings of 35th International ICSOBA Conference, Travaux No. 46*, Hamburg, Germany, October 2017, 2–5.
20. N. A. S. Webster et al., Predicting iron ore sinter strength through partial least square regression (PLSR) analysis of X-ray diffraction patterns. *Powder Diffraction.* Vol. 32, (2017), 66–69.
21. H. M. Silva et al., Geology, mining operation and scheduling of the Paragominas bauxite mine. *Proceedings of the 8th International Alumina Quality Workshop*. Darwin, Northern Territory, Australia. September 2008, 11–16.
22. Sijmen de Jong. SIMPLS: an alternative approach to partial least squares regression. *Chemometrics and Intelligent Laboratory Systems*. Vol. 18, (1993), 251–263.
23. S. Wold, Multivariate Data Analysis in Chemistry. in B. Kowalski (Ed.), *Chemometrics: mathematics and statistics in chemistry*. Reidel, Dordrecht, (1984), 17–95.
24. Yvonne M. Mos et al., X-ray diffraction of iron containing samples: the importance of a suitable configuratioin. *Geomicrobiology Journal*. Vol. 35, (2018), 511–517.
25. Mark G. Aylmore, Graham S. Walker. The quantification of lateritic bauxite minerals using X-ray powder diffraction by the Rietveld method. *Powder Diffraction,* Vol.13(03), (1998), 136–143.
26. S. P. A. Paz, et al, Synthesis, Rietveld refinement and DSC analysis of Al-goethite to support mineralogical quantification of gibbsitic bauxites. *J Therm Anal Calorim,* Vol. 128, (2017), 841–854.

Appendix

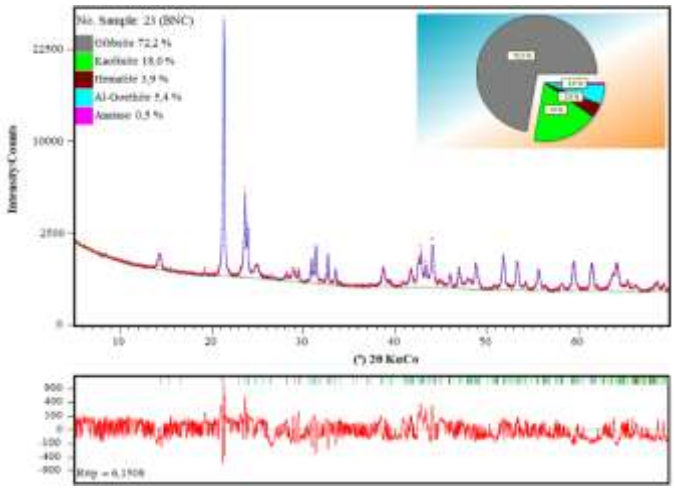

Figure 1A. Rietveld quantification of the bauxite sample no. 23 (BNC).

Table 1A. Outputs of the Rietveld refinement with its respective agreement indices.

		Replicate				
		1	**2**	**3**	**4**	**5**
BN	**Kaolinite**	25.3	24.9	24.4	24.3	23.6
	Rbragg	*2.57*	*2.57*	*2.94*	*2.84*	*3.26*
	Gibbsite	58.3	59.1	59.7	59.3	59.7
	Rbragg	*3.44*	*3.26*	*3.58*	*3.12*	*3.38*
	Hematite	9.3	9	8.8	9.1	8.8
	Goethite	6.6	6.6	6.6	6.9	7.4
	Anatase	0.5	0.4	0.4	0.4	0.5
	Rexp	*3.38*	*3.46*	*3.48*	*3.44*	*3.34*
	Rwp	*5.38*	*5.3*	*5.36*	*5.15*	*5.35*
	GOF	*1.58*	*1.53*	*1.55*	*1.49*	*1.6*
BNC	**Kaolinite**	18	19	18.9	17	15.5
	Rbragg	*3.94*	*4.52*	*4.71*	*4.11*	*4.99*
	Gibbsite	72.2	71.5	71.3	73.3	73.8
	Rbragg	*3.77*	*3.71*	*3.75*	*3.73*	*4.44*
	Hematite	3.9	3.9	3.9	4	4.2
	Goethite	5.4	5.1	5.5	5.2	6
	Anatase	0.5	0.5	0.4	0.5	0.5
	Rexp	*3.48*	*3.45*	*3.49*	*3.46*	*3.38*
	Rwp	*6.15*	*6.46*	*6.32*	*6.39*	*6.23*
	GOF	*1.76*	*1.87*	*1.81*	*1.84*	*1.84*
BC	**Kaolinite**	10.9	9.3	9	9.9	10.6
	Rbragg	*5.59*	*6.61*	*6.41*	*6.46*	*6.44*
	Gibbsite	76.4	76.6	77.5	77.2	75.9
	Rbragg	*1.95*	*3.26*	*2.31*	*2.11*	*4.57*
	Hematite	8.5	8.9	8.9	8.7	8.5
	Goethite	3.9	4.9	4.2	3.9	4.7
	Anatase	0.2	0.3	0.3	0.4	0.4
	Rexp	*3.13*	*3.18*	*3.21*	*3.18*	*3.05*
	Rwp	*7.89*	*8.07*	*7.48*	*9.24*	*9*
	GOF	*2.52*	*2.54*	*2.33*	*2.9*	*2.95*
BCBA	**Kaolinite**	20.2	19.9	18.1	18.9	19.3

Rbragg	*3.99*	*3.71*	*4.84*	*4.74*	*4.41*
Gibbsite	74.5	74.5	76.7	75.3	75.6
Rbragg	*2.55*	*2.51*	*2.54*	*2.42*	*2.93*
Hematite	2.4	2.1	2.1	2.3	2.3
Goethite	2.6	3.2	2.8	3.1	2.6
Anatase	0.4	0.3	0.3	0.4	0.3
Rexp	*3.35*	*3.27*	*3.32*	*3.3*	*3.13*
Rwp	*7.84*	*8.16*	*7.77*	*8.19*	*8.11*
GOF	*2.33*	*2.48*	*2.34*	*2.47*	*2.59*

Table 2A. Delta values from the calibration datasets obtained by cross-validation.

	Raw XRD data								Background subtracted							
	A		B		C		D		A		B		C		D	
	$AvAl_2O_3$	$RxSiO_2$	$AvAl_2O_3$	$RxSiO_2$	$AvAl_2O_3$	$RxSiO_2$	$AvAl_2O_3$	$RxSiO_2$	$AvAl_2O_3$	$RxSiO_2$	$AvAl_2O_3$	$RxSiO_2$	$AvAl_2O_3$	$RxSiO_2$	$AvAl_2O_3$	$RxSiO_2$
No.	**Delta**	**Delta**	**Delta**	**Delta**	**Delta**	**Delta**	**Delta**	**Delta**	**Delta**	**Delta**	**Delta**	**Delta**	**Delta**	**Delta**	**Delta**	Delta
1	0.235	-0.445	-0.009	-0.178	-0.066	-0.018	0.079	-0.02	0.274	-0.437	0.038	-0.113	0.386	-0.695	-0.016	-0.091
2	0.021	0.062	-0.013	-0.013	-0.049	0	-0.076	0.009	0.067	-0.015	0.06	0.116	-0.086	0.029	0.004	0.034
3	0.048	-0.091	0.031	-0.017	-0.216	0.043	-0.127	-0.027	0.073	-0.28	-0.123	0.084	-0.094	-0.384	0.014	0.048
4	-0.343	0.127	-0.128	0.144	-0.114	0.005	-0.277	0.034	-0.28	0.122	-0.185	0.088	-0.389	-0.029	-0.037	0.127
5	0.158	-0.033	-0.021	0.048	0.024	0.01	-0.047	0.027	0.181	0.041	0.095	0.017	0.146	0.006	0.019	0.013
6	-0.351	0.213	0.008	0.113	0.002	-0.031	-0.198	0.005	-0.068	0.055	-0.011	0.136	-0.304	0.237	-0.003	0.187
7	0.057	-0.03	0.029	-0.044	0.014	0.04	0.056	-0.043	0.223	0.114	-0.056	-0.004	0.245	0.312	-0.004	0.017
8	0.133	-0.149	-0.067	-0.09	-0.04	0.05	-0.153	-0.012	0.267	-0.124	-0.188	0.003	0.304	-0.082	0.005	0.042
9	-0.043	0.094	0.035	-0.049	0.082	-0.024	0.269	0.002	-0.12	-0.086	0.02	-0.038	-0.068	-0.047	-0.011	-0.047
10	0.208	-0.038	-0.016	-0.12	-0.049	-0.022	0.261	0.059	0.376	-0.274	-0.032	-0.116	0.316	-0.463	-0.003	-0.145
11	0.19	-0.12	0.048	-0.089	0.055	-0.007	0.167	-0.002	0.154	-0.175	0.217	0.057	0.079	-0.294	0.008	0.058
12	0.057	-0.079	-0.04	0.031	-0.024	0.03	0.005	-0.03	0.16	0.073	0.006	0.056	0.009	0.097	0.011	0.056
13	0.188	-0.113	0.049	-0.114	0.188	-0.019	0.366	0.028	0.053	-0.117	0.059	0.107	0.197	-0.044	0.026	0.054
14	0.073	-0.027	-0.07	0.098	0.044	0.052	-0.063	0.057	-0.081	0.286	0.106	0.037	-0.306	0.399	0.002	0.007
15	-0.149	-0.012	-0.065	-0.028	0.003	-0.027	-0.177	-0.031	0.009	0.336	-0.298	0.071	-0.024	0.369	-0.01	0.042
16	-0.142	0.048	-0.035	0.117	-0.093	-0.043	-0.292	-0.006	-0.138	0.158	-0.29	0.032	-0.218	0.247	0.003	-0.003
17	-0.372	0.234	-0.033	-0.113	0.011	-0.048	-0.092	-0.018	-0.333	-0.513	0.099	-0.18	-0.034	-0.644	-0.009	-0.103
18	-0.174	0.169	-0.013	0.177	-0.071	0.006	0.001	0.048	0.034	0.147	0.084	-0.007	-0.145	0.138	-0.021	0.086
19	-0.143	0.123	0.034	-0.056	0.125	-0.022	0.006	-0.01	-0.474	-0.139	0.233	0.009	-0.239	-0.274	0.007	-0.059
20	0.132	-0.008	0.054	0.09	0.107	0.032	0.175	-0.031	-0.071	0.186	0.161	-0.04	-0.036	0.131	0.009	-0.136
21	-0.015	-0.21	0.034	-0.049	0.016	0.033	-0.075	-0.034	-0.287	0.056	0.068	-0.052	-0.153	0.085	0.001	-0.083
22	0.249	-0.047	-0.007	0.079	0.096	-0.019	0.215	0.019	0.208	-0.268	0.072	0.017	0.362	-0.387	0.004	0.122
23	0.104	-0.024	-0.054	-0.159	-0.034	-0.057	0.027	0.048	-0.024	-0.364	-0.058	-0.134	0.305	-0.422	-0.014	-0.008
24	0.103	-0.069	0.101	-0.082	-0.06	0.026	-0.011	-0.092	0.12	0.158	-0.023	-0.011	-0.058	0.186	0.022	-0.033
25	0.165	-0.216	-0.011	-0.059	-0.015	-0.056	-0.244	-0.045	0.47	-0.338	0.037	-0.126	0.368	-0.221	-0.025	0.047
26	-0.314	0.234	-0.008	-0.026	-0.114	0.019	-0.069	0.009	-0.433	0.403	-0.117	0.048	-0.434	0.514	0.007	-0.052

27	0,003	-0,101	-0,009	-0,112	0,052	0,007	-0,132	0,009	-0,299	0,147	-0,142	0,008	-0,13	0,176	0,002	0,081
28	-0,046	0,261	0,03	0,144	0,022	0,024	0,07	0,027	-0,108	0,421	-0,054	0,143	-0,031	0,577	-0,007	0,096
29	0,059	0,209	0,099	0,121	0,104	0,012	0,168	-0,008	0,101	0,183	0,193	0,119	0,191	0,253	0,012	0,043
30	-0,019	0,012	0,035	0,124	0,032	-0,019	0,216	0,048	0,018	-0,027	0,022	-0,177	-0,056	0,003	-0,001	-0,286
31	-0,071	0,027	0,012	0,115	-0,034	0,024	-0,048	-0,019	-0,074	0,271	0,005	-0,15	-0,104	0,225	0,006	-0,113